TURBULENT INTERFACIAL BOUNDARY CONDITIONS FOR SPILLING BREAKERS

Shubhra K. Misra [1], Maurizio Brocchini [2] and James T. Kirby [3]

This paper presents experimental observations as well as theoretical formulations of the flow structure in the turbulent shear layer in spilling breakers. The theoretical model is developed within the framework of a three-layer system, with the top layer being the two-phase (air/water) turbulent surface layer, and the bottom layer comprising the single phase (water) irrotational flow. The model development in the single phase (water) turbulent shear layer is guided by and validated with PIV flow measurements of a turbulent hydraulic jump. The breaker shear layer is seen to resemble a classical mixing layer with entrainment of fluid into the reverse flow region localized about the mean surface. Preliminary results are reported on interfacial boundary conditions which account for the contributions from the surface layer as well as the evolution of turbulent and mean quantities in the breaker shear layer. Such interfacial boundary conditions can be incorporated into Reynolds-averaged Navier-Stokes numerical models for simulating the spatio-temporal evolution of the turbulent and mean flow in spilling breakers.

1. INTRODUCTION

An accurate modeling of turbulence generated by breaking waves is essential in fully understanding and simulating the complicated mechanisms of mass, momentum, and energy transfer from organized wave motion to nearshore current and sediment suspension and transport processes in the surf-zone. There are few theoretical and experimental studies which provide a detailed spatial description or a fundamental understanding of the temporal evolution of the mean and turbulence flow in the breaker (Duncan, 2001). Non-intrusive experimental methods such as particle image velocimetry (PIV) and video based imaging techniques have contributed significantly to a better qualitative and quantitative understanding of the instantaneous and mean flow structure (Lin and Rockwell, 1995; Govender *et al.*, 2002). Motivated by these observations, simplified theoretical models have been formulated to describe the flow in the breaker (Longuet-Higgins and Turner, 1974; Cointe and Tulin, 1994). In the hydraulic jump/bore model of Madsen and Svendsen (1983), which provided motivation for the

[1]HALCROW HPA, 22 Cortlandt Street, 33rd Floor, New York, NY 10036, USA
[2]Istituto di Idraulica e Infrastrutture, Viarie, Universit Politecnica delle Marche, Via Brecce Bianche, 60131 Ancona, Italy
[3]CACR, University of Delaware, Newark, DE 19716, USA

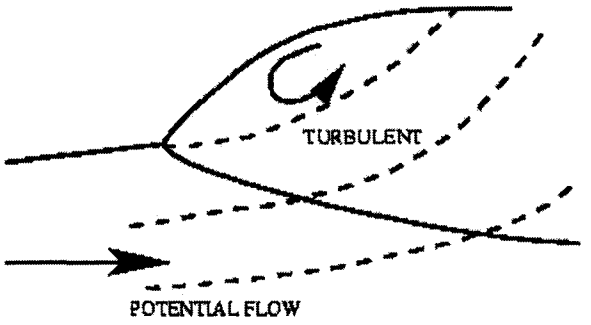

Figure 1: Schematic representation of the hydraulic jump/bore model. Adapted from Madsen and Svendsen (1983).

development of the present theoretical model, the turbulence was assumed to spread downstream in a wedge originating at the toe of the breaker front (Figure 1). The turbulence was modeled by a simplified $k-\epsilon$ model allowing for non-equilibrium in the turbulent kinetic energy.

The theoretical models mentioned above have primarily been "bulk" formulations, neglecting various details of the flow structure. The underlying assumptions in these studies are that of a generally accepted conceptual description of the breaker shear layer as a mixing layer with or without a recirculating roller which, however, remain unquantified and unformulated in the details of their structure and interaction with each other or the rest of the flow. In particular, the effects of the two-phase surface layer have not been paid much attention. In recent years, with a steady increase in computational resources facilitating a more accurate numerical modeling of the two-phase surface turbulence, heterogenous domain decomposition techniques have been used to separately model the viscous breaker region and the irrotational flow underneath, where a critical component of the coupling is the mean pressure at the interface (Rhee and Stern, 2002; Iafrati and Campana, 2005). This paper is aimed at formulating such interfacial boundary conditions from a rigorous theoretical description of the flow aided by high-resolution measurements of the flow in a spilling breaker.

In section 2, laboratory PIV experiments for an air-entraining weakly turbulent hydraulic jump are described. The underlying framework and assumptions of the theoretical formulation are discussed and validated with the PIV measurements in section 3 and the interfacial boundary conditions are highlighted. Conclusions and discussions are presented at the end of the paper in section 4.

2. LABORATORY MEASUREMENTS OF A TURBULENT HYDRAULIC JUMP

Turbulent hydraulic jumps fall under the general category of steady spilling breakers such as those generated by submerged hydrofoils (Duncan, 2001). In similtude with saturated surf-zone breakers, the upstream Froude number (Fr) is found to be in the range 1.15 to 1.26. For such low Froude number turbulent jumps, the energy dissipation in the transition region from supercritical to subcritical flow comes primarily from sheared turbulence accompanied by free surface air-entrainment. The most comprehensive experimental study to date of low Froude number, weakly turbulent jumps with breaking and air entrainment is that of Svendsen *et al.* (2000). They found that, contrary to the traditionally simplified formulations of a hydraulic jump, the effects of non-uniform velocities and non-hydrostatic pressure are important for mass and momentum conservation. Little attention was focused on the intermittency of the surface and its influence on the flow structure. A single roller was found to reside in the region bounded from below by, what the authors referred to as, a dividing streamline (above which the net volume flux was zero), and from above by the mean surface.

The PIV measurements discussed in this paper are of a laboratory generated turbulent hydraulic jump with breaking and air entrainment. The upstream to downstream depth ratio was 1.25, and the upstream Froude number was 1.2. Details of the experimental set-up and flow parameters can be found in Misra (2005). A non-intrusive detection of the instantaneous air-water interface from the raw PIV images was achieved through sophisticated image processing algorithms (Misra *et al.*, 2005) and the instantaneous velocities were computed using a phase-correlation based hierarchial, multi-pass motion estimation algorithm that has been extensively tested with ground-truth measurements (Thomas *et al.*, 2005). 1020 image pairs were collected and mean and root mean square turbulent quantities were calculated using suitable conditional averaging techniques (Misra *et al.*, 2005).

Figure 2 shows that the surface-normal velocity is nearly zero in the reverse-flow region. The flow is from left to right, and the toe of the breaker is at $\tilde{x} = \frac{\mathrm{x}}{h_0} \sim 0.47$, where x is the streamwise coordinate and h_0 is the upstream water depth. y is the vertical coordinate and the origin of the coordinate system is defined at the flume bottom at an arbitrary upstream (of the toe) location. There are large, positive values of surface normal velocity, $\hat{V}_n$, below the mean surface and are an indication of the entrainment of water from below. It is also clear from the present data that, though most

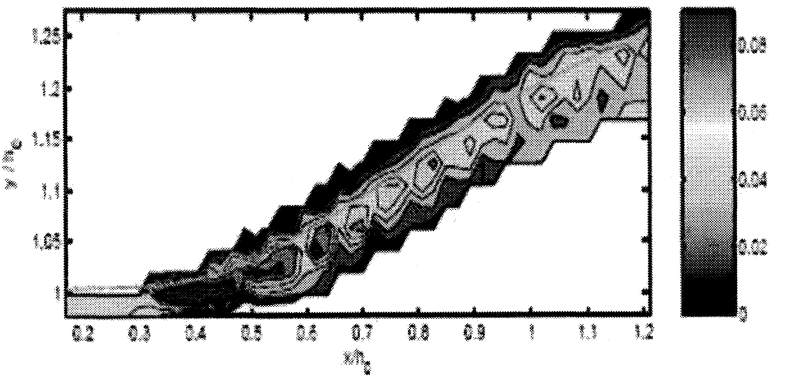

Figure 2: Mean surface-normal velocity $\hat{V}_n$ (m/s). Solid line is the ensemble-averaged free surface.

of the entrainment occurs near the toe, inflow from below occurs all over the reverse-flow region with approximately equidistant peaks of upwelling. As opposed to the assumption made by IS00, the mean shear is finite and negative at the mean surface. The present topology of the reverse-flow region is different from the concept of an isolated recirculating eddy/'roller' bounded on the top by a mean surface and on the bottom by a dividing streamline, since there clearly is reverse flow above the mean surface. As noted by Banner and Phillips (1974), we believe it essential to replace the idea of a mean surface in the reverse-flow region by an intermittency zone, which in the present measurements, is taken into account through the conditional averaging technique applied to the fluctuating air-water interface; the fluctuations follow a Gaussian distribution (Misra *et al.*, 2005).

It is fairly well-established that there is an intense shear layer formed below a fully-formed, quasi-steady spilling breaker, which spreads downstream from the foot of the breaker, and qualititave observations have suggested this to be a "mixing layer" (Peregrine and Svendsen, 1978; Hoyt and Sellin, 1989). Lin and Rockwell (1995) had found coherent vortical motions, and concentrated vorticity along a "mixing layer" originating from the toe. However, there has been no detailed experimental evidence for the suggested classification of the shear layer in a fully-formed breaker as a mixing layer. Figure 3 shows the Reynolds shear stress in the breaker shear layer of the hydraulic jump. The Reynolds shear stress is negative throughout the shear layer, implying an upward diffusion of momentum. The Reynolds shear stress has its largest value at $\tilde{x} \sim 0.59$, $\tilde{y} \sim 1$, downstream of the toe.

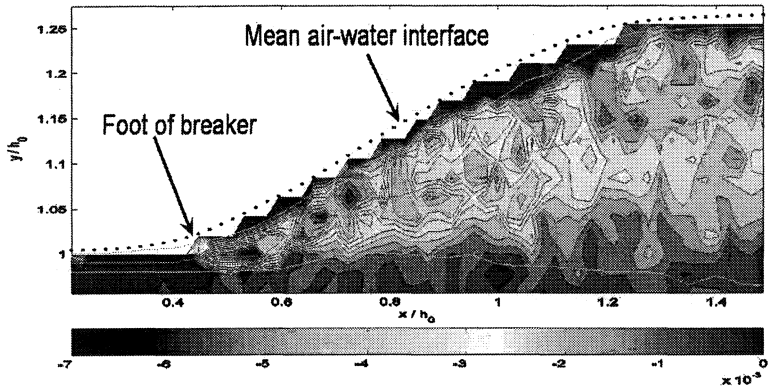

Figure 3: Reynolds shear stress, τ' (m^2/s^2) in the mixing layer. The dotted line is the mean surface and the thin solid white lines in the mixing layer represent 10 % of the maxima of the Reynolds stress.

The width of the mixing layer, W, is calculated and made dimensionless with h_0 and is shown in Figure 4 along with the linear least squares regression fit. In terms of the absolute coordinate $\tilde{x}$, there is a linear increase in the width till about $\tilde{x} \sim 1.2$, after which it becomes approximately constant and the flow resembles a wake. This is in good qualitative agreement with the spreading rate of mixing layers where the "wedge" is known to spread in a linear fashion and indicates that the breaker shear layer can be classified as a mixing layer with its origin downstream of the toe and extending downstream till it changes to a wake-type flow. This transition occurs at approximately the location of the peak negative curvature of the mean free surface. Therefore, the breaker shear layer is seen to resemble a plane mixing layer. The mean value of the non-dimensional growth rate in the mixing layer ($\approx$0.29) is found to be in good agreement with values found earlier by Brown and Roshko (1974).

3. THEORETICAL MODEL FOR SPILLING BREAKERS

Partially motivated by the measurements, a comprehensive theoretical model has been developed for the description of turbulence in the shear layer of unsteady spilling breaking waves by extending the formulations in Brocchini and Peregrine (2001a,b) and Brocchini (2002). The governing equations have been formulated within the framework of a three-layer system (see Figure 5) in which the top layer represents the intermittent effects of two-phase free-surface turbulence (Brocchini, 2002) and the bottom layer is assumed to be irrotational. The middle layer is the single phase

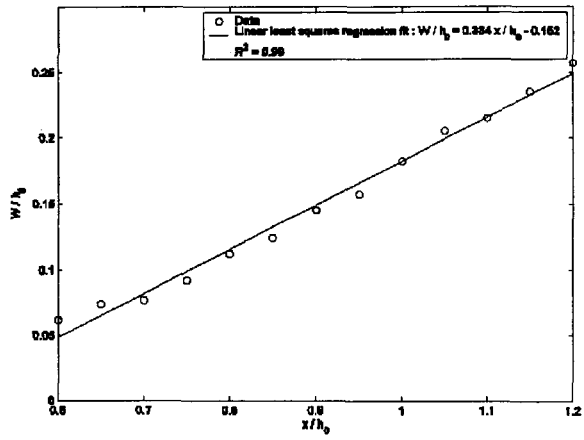

Figure 4: Streamwise variation of the width of the mixing layer. Measurements (circles) and linear regression fit (solid line).

mixing layer in which turbulence is generated due to the continuous shearing action of the flow downstream of the toe of the breaker. In a mobile coordinate system (s, n), equations of mass and linear momentum in the turbulent thin layer in covariant form are derived including a correct representation of two-phase flow near the surface, streamline and geometric curvature, unsteadiness, non-hydrostatic pressure, and local rotation which are all inherent to the dynamics of the layer of turbulent flow. Turbulent averaging leads to Reynolds-type equations. A k-ϵ closure for Reynolds stresses based on Boussinesq eddy viscosity concept is used and a transport equation allows for non-equilibrium of the turbulent kinetic energy.

These contributions give a complete account of the motion of the unsteady spilling breaker. They also make these equations very complex and the solution of the complete equations a very difficult task. Scaling arguments are adopted to retain only the most important terms in the basic equations and to help compare relative weights of terms appearing in different equations. As is well known, mixing layers (or shear layers) are characterized by a scale velocity $\tilde{U}$ for the cross-stream (n) variation of the mean velocity component in the streamwise direction $(\hat{\mathbf{s}})$. A first useful relationship which characterizes the flow in the turbulent layer expresses the observation that the layer is thin, i.e., the thickness, b, is much smaller than the streamwise length scale, L:

$$b \ll L \quad \text{or} \quad \frac{b}{L} = \epsilon \ll 1. \tag{1}$$

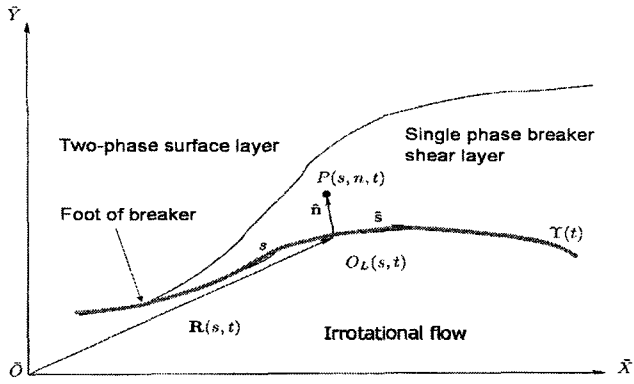

Figure 5: Global geometry adopted in the model for the system wave - turbulent thin layer - surface layer.

L represents the size of the region of the wave with the highest curvature. From the present measurements, considering the variation of the calculated length scale of the mixing layer, values of ϵ, the geometric parameter, averaged over the breaker shear layer are of the order of 0.03, which is slightly smaller than typically observed values of order 0.06 for jets and mixing layers (Tennekes and Lumley, 1972). These values are reasonable enough to satisfy the 'thin layer' approximation.

We also introduce a dimensionless kinematic parameter μ which represents the ratio of the scales for turbulent velocities and mean velocities, and use it to implicitly estimate the size of the different contributions in the following analysis:

$$\mu = \frac{\tilde{u}}{\tilde{U}}\ , \qquad \mathcal{O}(\epsilon) < \mu < \mathcal{O}(1). \tag{2}$$

In the following, when referring to the leading order or $\mathcal{O}(1)$ model, the contributions of terms of $\mathcal{O}(\epsilon)$ and higher are neglected. Also, the particular flow regime analyzed is made explicit depending on the size of μ. For example, at the leading edge of the breaker, where intense turbulence is generated by the shear induced by the flow separation, turbulent velocities are of the same order as the mean velocities, and $\mu \sim \mathcal{O}(1)$, whereas in the far wake region, $\mu \sim \mathcal{O}(\epsilon)$.

Similar to Madsen and Svendsen (1983), a cubic polynomial is used for the cross-flow profile for the mean horizontal velocity. In a significant difference from their model, the two-phase surface layer contributions are taken

into account by enforcing the kinematic free surface boundary condition at the top of the single phase shear layer, and using the results obtained in Brocchini and Peregrine (2001b) and Brocchini (2002). The other matching conditions used to solve for the flow are continuity of mean velocity at the top and bottom of the layer and vanishing turbulent shear stresses at the interface with the irrotational flow underneath. The mean streamwise velocity is given by

$$U(s,\sigma,t) = \hat{U} + (U_b - \hat{U})\sigma^2 + A\left[U_b - \hat{U} - b(s)\Omega\right]\sigma^2(1-\sigma), \qquad (3)$$

where U_b and $\hat{U}$ are the mean velocities at the bottom and top of the layer respectively, $\sigma = \frac{n}{b}$ is a non-dimensional vertical coordinate, Ω denotes the rotation and A is the coefficient of the cubic term and represents the mean shear at the interface with the surface layer. For $\Omega = 0$, this reduces to

$$U(s,\sigma,t) = \hat{U} + (U_b - \hat{U})\sigma^2[1 + A(1-\sigma)]. \qquad (4)$$

The analytical solution for the mean horizontal velocity can be checked using the present measurements. A cubic polynomial was fit to the measured values for U. This is shown as the blue solid line in Figure 6. The coefficient of the cubic term (A) was calculated from the fit and is shown at each horizontal location. Once A had been calculated, by approximating $\hat{U}$ and U_b with the mean horizontal velocity values at the bottom and top (at the contours for 10 % of the maximum Reynolds shear stress; see Figure 3) of the mixing layer, the mean horizontal value at each vertical location was calculated from equation (4), and this is shown as the red line in the figure. Because of the small thickness of the shear layer near the toe, few data points were available for a robust fit to the profile. Therefore, the streamwise locations were chosen in the middle part of the shear layer. Equation (4) is seen to provide a good approximation to the vertical variation of the mean horizontal velocity in the shear layer.

Using the profiles for the mean and turbulent quantities, the leading order equations are analytically integrated across the width of the layer. The leading-order contributions from the normal component of the momentum equation are essentially a balance between the normal turbulent stress and the normal mean pressure gradient. Using the profiles for the normal turbulent stresses and the turbulent kinetic energy, this can be integrated across the layer from $n = 0$ to $n = b$ to give

$$P_0 = P_b + 2\rho C_3 \Lambda^2 f^2 \left[(-A+2)\left(-A+2+\frac{2b\Omega}{f}\right)\right]. \qquad (5)$$

Λ denotes the ratio of turbulence production and dissipation, f denotes the streamwise variation of the flow, ρ the density, and C_3 is a constant of the

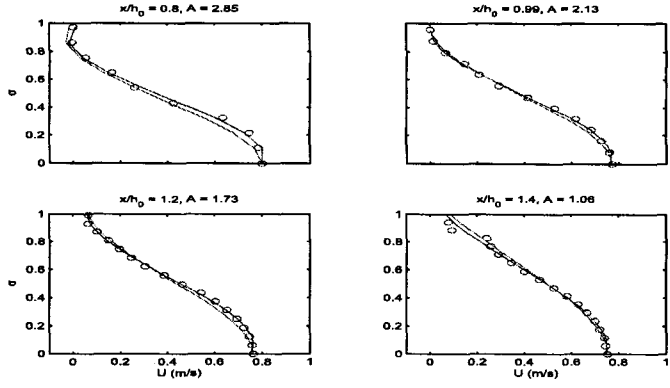

Figure 6: Cubic profile fit (blue solid line) for mean horizontal velocity data (circles). Red line is the estimated mean velocity from equation (4). σ is the non-dimensional vertical coordinate.

turbulence model. P_0 and P_b are respectively the pressure at the bottom and top of the layer, and P_b can be obtained from the dynamic boundary condition derived in Brocchini and Peregrine (2001b) (see their equation (5.19)) which includes the surface layer contributions. Note the presence of extra pressure with respect to P_b due to rotation and non-zero mean shear stress (represented by $A \neq 2$) at the top of the layer. Note that the effect of gravity is absent at leading order and is only felt at $(O(\epsilon))$. The normal turbulent stresses make a dominant contribution to the non-hydrostatic component of the pressure. In the absence of rotation and mean shear at the top of the layer ($\Omega = 0$ and $A = 2$), $P_0 = P_b$. In other words, there is uniform pressure across the layer. On integrating the $\mathcal{O}(1)$ contributions from the streamwise momentum equation,

$$\hat{\mathbf{n}} \cdot \frac{\partial \mathbf{R}}{\partial t} = \frac{C_t \Lambda f^2 (2 - A) \left[A - \left(2 + \frac{2b\Omega}{f} \right) \right]^2}{\left(U_b - \hat{U} \right)}, \tag{6}$$

which describes the unsteady vertical motion of the layer. Note that the steady state is recovered for $A = 2$ which represents vanishing mean shear stress at the surface.

The normal integration of the $\mathcal{O}(1)$ turbulent kinetic energy equation results in an expression for $\Lambda(s)$ describing the local imbalance between

production and dissipation is found. In the absence of rotation,

$$\Lambda^2(s) = \frac{-6A^3 + 63A^2 - 126A + 210}{105(2-A)^3\left[(2-A)^2 - 4\frac{(1-2A)}{(2-A)} + \frac{C_\varepsilon}{C_t}\right]}. \tag{7}$$

C_ε and C_t are constants in the turbulence model (Launder and Spalding, 1972). The first thing to note in the above expression is the singularity at $A = 2$. Since Λ^2 is the dissipation divided by the production, near the leading edge of the breaker, $\Lambda^2 < 1$. The singularity appears when the production vanishes, and this is expected to occur in the downstream direction. In contrast to Madsen and Svendsen (1983), where A is a constant (chosen as a best-fit to data), $A(s)$ in the present model varies in the streamwise direction, and its variation can be modeled in terms of the dynamics of the turbulence near the foot of the breaker. The streamwise dependence follows from the more complex flow situation analyzed here (e.g. non-hydrostatic pressure, vertical accelerations, etc.) with respect to those of Madsen and Svendsen (1983).

Instead of using the profiles for the mean and turbulent quantities, the integration of the governing equations across the layer can also be done by defining layer-averaged variables with the aim of developing a model which, apart from its governing variables, is determined entirely by the information provided from the underlying flow so that the integrated equations also serve as boundary conditions for the irrotational flow below. The variables for the model are the layer thickness, b, the layer-averaged mean horizontal velocity, $\overline{U} \equiv \frac{\int_0^b U dn}{b}$, and the layer-averaged turbulent kinetic energy, $\overline{k} \equiv \frac{\int_0^b k dn}{b}$. The analysis assumes $\Omega = 0$. The layer-averaged equations for conservation of mass, momentum and turbulent kinetic energy are given as

$$\frac{\partial b}{\partial t} + C_B\frac{\partial b}{\partial s} + C_U\frac{\partial \overline{U}}{\partial s} + C_K\frac{\partial \overline{k}}{\partial s} = C_R, \tag{8}$$

$$\frac{\partial \overline{U}}{\partial t} + M_B\frac{\partial b}{\partial s} + M_U\frac{\partial \overline{U}}{\partial s} + M_K\frac{\partial \overline{k}}{\partial s} = M_R, \quad \text{and} \tag{9}$$

$$\frac{\partial \overline{k}}{\partial t} + K_B\frac{\partial b}{\partial s} + K_U\frac{\partial \overline{U}}{\partial s} + K_K\frac{\partial \overline{k}}{\partial s} = K_R, \tag{10}$$

or in matrix form as

$$\begin{Bmatrix} b \\ \overline{U} \\ \overline{k} \end{Bmatrix}_t + \begin{bmatrix} C_B & C_U & C_K \\ M_B & M_U & M_K \\ K_B & K_U & K_K \end{bmatrix} \begin{Bmatrix} b \\ \overline{U} \\ \overline{k} \end{Bmatrix}_s = \begin{bmatrix} C_R \\ M_R \\ K_R \end{bmatrix},$$

where the subscripts denote partial differentiation with respect to the variables, and the coefficients are functions of the dependent variables. The

above system of equations can either be regarded as a description for the turbulent dynamics in the thin layer, or as turbulent free surface boundary conditions for the irrotational flow below. The two flows are coupled through the mass exchange and pressure at the boundary. The mass exchange is represented by the mean velocities, V_0 and $\hat{U}$. The layer-averaged pressure ($\overline{P}$) and the pressure at the top of the layer (P_b) can easily be expressed in terms of the layer-averaged turbulent kinetic energy, $\overline{k}$. Since a consistent set of equations for the $O(\epsilon)$ model has contributions from the $O(1)$ normal momentum equation, using the $O(1)$ relationship between the normal turbulent stress and the turbulent kinetic energy, the pressure at the base of the layer, for the $\mathcal{O}(\epsilon)$ model, is given by

$$P_0 = P_b + 2\rho C_3(k_b - k_0), \tag{11}$$

where k_b and k_0 represent the turbulent kinetic energies at the bottom and top of the shear layer. Since the diffusion of turbulent kinetic energy at the bottom has been neglected, in the absence of rotation, the profile for the turbulent kinetic energy gives $k_0 = 0$. Also, since k_b is related to $\overline{k}$ through $k_b = A_k\overline{k}$ (A_k represents the coupling between the surface layer and the single phase turbulent layer), and $P_b = \rho C_p\overline{k}$, the pressure at the base of the layer, and as a boundary condition for the irrotational flow is found to be

$$P_0 = \overline{k}\rho(C_p + 2C_3A_k). \tag{12}$$

Therefore, solving the evolution equation for the layer-averaged turbulent kinetic energy, yields the solution for the pressure at the base of the layer, which is used in the dynamic boundary condition (the Bernoulli equation) to solve for the potential flow underneath (Iafrati and Campana, 2005).

4. CONCLUSIONS

PIV measurements were used to provide a detailed picture of the mean and turbulent structure of an air-entraining hydraulic jump set up in Froude similitude with surf-zone breakers. The traditional concept of a roller in the form of a recirculating region is seen to be only a partial description of the mean flow near the interface, since along with a weak downslope flow above the mean surface, there is mass exchange with the underlying flow across the lower boundary of the roller. The turbulence structure of the breaker shear layer is seen to resemble that of a mixing layer originating at the foot of the breaker followed by a wake further downstream. The average growth rate is in good agreement with observed values in typical mixing layers. Model equations for a comprehensive description of the flow in the breaker shear layer have been developed, including non-hydrostatic and unsteady effects, streamline and geometric curvature, rotation and the effects of surface turbulence. The geometric and kinematic scaling assumptions are justified

from the present measurements. The vertically integrated model provides evolution equations for the mean and turbulent flow, as well as the motion of the interface. The mean shear at the top of the layer significantly affects the mean and turbulent flow in the layer. Experimental results validate the assumed classification of the breaker shear layer as a classical mixing layer and the vertical profiles of the mean velocity in the mixing layer are found to be in good agreement. The layer-averaged equations are coupled to the underlying flow through mass entrainment and excess pressure at the interface, and they serve as boundary conditions for the flow below and can be used in Reynolds-averaged Navier-Stokes numerical models to describe the evolution of the flow in the shear layer of a spilling breaker.

ACKNOWLEDGEMENTS

A substantial part of this research has been funded by the National Oceanographic Partnership Program (NOPP) grant number N00014-99-1-1051. Part of this research was funded by the University of Genoa and the College of Marine Studies, University of Delaware. Prof. D. H. Peregrine's contributions in the theoretical development of the model are gratefully acknowledged. SKM acknowledges the travel and conference registration support provided by HALCROW HPA.

References

Banner, M. L. and Phillips, O. M. (1974). On the incipient breaking of small scale waves. *J. Fluid Mech.*, **65**, 647–656.

Brocchini, M. (2002). Free surface boundary conditions at a bubbly/weakly-splashing air-water interface. *Phys. Fluids*, **14**(6), 1834–1840.

Brocchini, M. and Peregrine, D. H. (2001a). The dynamics of turbulent free surfaces. part 1. Description. *J. Fluid Mech.*, **449**, 225–254.

Brocchini, M. and Peregrine, D. H. (2001b). The dynamics of strong turbulence at free surfaces. part 2. Free-surface boundary conditions. *J. Fluid Mech.*, **449**, 255–290.

Brown, G. L. and Roshko, A. (1974). On density effects and large structures in turbulent mixing layers. *J. Fluid Mech.*, **64**, 775–816.

Cointe, R. and Tulin, M. P. (1994). A theory of steady breakers. *J. Fluid Mech.*, **276**, 1–20.

Duncan, J. H. (2001). Spilling breakers. *Ann. Rev. Fluid Mech.*, **33**, 519–547.

Govender, K., Mocke, G., and Alport, M. (2002). Video imaged surf zone wave and roller structures and flow fields. *J. Geophys. Res.*, **107**(C10), 3177.

Hoyt, J. W. and Sellin, R. H. J. (1989). Hydraulic jump as "Mixing layer". *J. Hyd. Engrng.*, **115**(12), 1607–1614.

Iafrati, A. and Campana, E. F. (2005). Free-surface fluctuations behind microbreakers: space-time behaviour and subsurface flow field. *J. Fluid Mech.*, **529**, 311–347.

Launder, B. E. and Spalding, D. B. (1972). *Mathematical models of turbulence*. Academic Press, London and New York.

Lin, J. C. and Rockwell, D. (1995). Evolution of a quasi-steady breaking wave. *J. Fluid Mech.*, **302**, 29–44.

Longuet-Higgins, M. S. and Turner, J. S. (1974). An entraining plume model of a spilling breaker. *J. Fluid Mech.*, **63**, 1–20.

Madsen, P. A. and Svendsen, I. A. (1983). Turbulent bores and hydraulic jumps. *J. Fluid Mech.*, **129**, 1–25.

Misra, S. K. (2005). *The turbulent dynamics of quasi-steady spilling breakers - Theory and experiments*. Ph.D. thesis, University of Delaware.

Misra, S. K., Thomas, M., Kambhamettu, C., Kirby, J. T., Veron, F., and Brocchini, M. (2005). Estimation of complex air-water interfaces from PIV images. *Exp. Fluids*, **40**(5), 764–775.

Peregrine, D. H. and Svendsen, I. A. (1978). Spilling breakers, bores and hydraulic jumps. In *Proceedings of the 16th ICCE, Hamburg*, pages 540–555. ASCE.

Rhee, S. H. and Stern, F. (2002). RANS model for spilling breaking waves. *J. Fluids Engrng.*, **124**, 424–432.

Svendsen, I. A., Veeramony, J., Bakunin, J., and Kirby, J. T. (2000). The flow in weak turbulent hydraulic jumps. *J. Fluid Mech.*, **418**, 25–57.

Tennekes, H. and Lumley, J. L. (1972). *A first course in turbulence*. MIT Press.

Thomas, M., Misra, S. K., Kambhamettu, C., and Kirby, J. T. (2005). A robust motion estimation algorithm for PIV. *Meas. Sci. and Tech.*, **16**(3), 865–77.